EVALUATING A POWER GRID'S VULNERABILITY TO HIGH ALTITUDE ELECTROMAGNETIC PULSES USING DETAILED EARTH CONDUCTIVITY MODELS

A Thesis

by

RAYMUND HAN-WEN LEE

Submitted to the Office of Graduate and Professional Studies of
Texas A&M University
in partial fulfillment of the requirements for the degree of

MASTER OF SCIENCE

Chair of Committee,	Thomas Overbye
Co-Chair of Committee,	Katherine Davis
Committee Members,	Robert Nevels
	Nicholas Suntzeff
Head of Department,	Miroslav Begovic

December 2018

Major Subject: Electrical Engineering

ABSTRACT

A nuclear bomb detonated above the earth's surface can cause a high-altitude electromagnetic pulse (HEMP). HEMPs create an electric field at the earth's surface, which induces unwanted slowly varying dc currents, called geomagnetically induced currents (GIC) on transmission lines. The magnitude of the electric field highly depends on the conductivity of the earth, hundreds of thousands of meters below the surface. The earth's conductivity is very complex and there exist different models to represent it. HEMP electric fields are commonly evaluated using a simple model called the uniform model, which models the earth using a single value of conductivity. This thesis describes a method to convert HEMP electric fields under a more detailed conductivity model, called the 1D model, which is based on geological surveys and includes regional variations. Using the 1D model enables locationally dependent simulations of HEMP electric fields, yielding more realistic results. This methodology has been automated by a tool, created with MATLAB, and was applied to several publicly available HEMP electric field waveforms at different locations across the continental United States. These electric fields are analyzed by comparing their magnitudes and their impact on a 10,000-bus synthetic grid. The results show the extent that HEMP electric field magnitudes can vary from region to region. Also, evaluations of different HEMP electric field waveforms show that each waveform may have characteristics that impact the grid differently. Based on the analysis performed in this thesis, it is recommended that comprehensive HEMP vulnerability studies utilize multiple worst-case HEMP waveforms while considering regional differences in earth conductivity.

ACKNOWLEDGMENTS

Most of all, I would like to thank Dr. Overbye for providing me with many opportunities to learn throughout my time at Texas A&M. Under his guidance, I gained many new skills while contributing research toward a fascinating topic. My knowledge and passion for power engineering has grown a lot throughout my graduate experience largely due to Dr. Overbye's mentorship, and I feel very fortunate to have been his student.

I would also like to thank my wonderful girlfriend, Hanyue, for her selfless support as we endured through the challenging parts of graduate school together. With her, the long nights spent writing papers and studying for tests were enjoyable. When I look back at my time at Texas A&M, I will remember a time of happiness because of her.

I also want to also acknowledge the Texas A&M rock climbing community for making the time I spent outside of the office enjoyable. I couldn't have asked for a better way to relax after work than having this close-knit group of motivated climbing partners with whom I trained.

Lastly, I would like to thank my mother and father for stressing the value of an education in my upbringing and for their endless support in all my pursuits.

CONTRIBUTORS AND FUNDING SOURCES

Contributors

This work was supervised by a thesis committee consisting of Professor Thomas Overbye [advisor], Professor Katherine Davis [co-advisor], and Professor Robert Nevels of the Department of Electrical and Computer Engineering and Professor Nicholas Suntzeff of the Department of Physics and Astronomy.

All work for the thesis was completed by the student, in collaboration with Adam Birchfield, Komal Shetye, and Dr. Thomas Overbye of the Department of Electrical and Computer Engineering.

Funding Sources

I would like to acknowledge the Bonneville Power Administration for primarily funding my research and master's education under project TIP-359. Funding was also provided by the National Science Foundation (NSF) under award number NSF 15-20864.

TABLE OF CONTENTS

Page

LIST OF FIGURES

Page

LIST OF TABLES

Page

1. INTRODUCTION AND MOTIVATION*

Geomagnetic disturbances (GMD) and high-altitude electromagnetic pulses (HEMP) are two phenomena that are known to negatively impact the power grid by inducing unwanted currents throughout the system, called geomagnetically induced currents (GIC). A GMD or HEMP can potentially affect millions of square kilometers and cause widespread blackouts and damage to the electrical infrastructure. Because of this, GMDs and HEMPs have been categorized as high-impact low-frequency (HILF) events by the North American Electric Reliability Council (NERC) [1]. The Northeastern blackout of 2003 dramatically showed that human society relies on the uninterrupted operation of the electrical power grid for basic needs such as transportation and communication. As technology advances and society's reliance on electricity increases, it is increasingly important to understand the impact of GMDs and EMPs on the bulk power system.

A GMD occurs when charged particles ejected from a coronal mass ejection reach the earth. Historically, the amount of solar activity has followed a cyclical pattern, peaking about every 11 years [2]. The electric field resulting from a solar storm can be characterized by magnitudes up to tens of volts per kilometer (V/km) and durations that can be measured in hours. A GMD event in 1989 resulted in a widespread blackout of the Quebec grid for about nine hours, motivating the power industry to understand GIC-related phenomena better [3]. More extreme GMD storms were observed in 1859 and 1921, however, the effects of these storms on the electric grid were less significant because the electric grid was not as developed at the time of these storms [4].

HEMPs are caused by nuclear bombs detonated tens to hundreds of kilometers above the earth's surface. Much of what is publicly known about the characteristics of a HEMP electric field was observed during nuclear bomb experimentation between World War II and the early 1960's. In 1962, the data collected from an experiment conducted over the Pacific Ocean named Starfish Prime significantly raised the understanding of the effects of a high-altitude nuclear detonation. This experiment also increased public awareness of this phenomenon by damaging streetlights in Honolulu, Hawaii [5]. In 1963, the United States, Soviet Russia, and the United Kingdom signed a treaty, banning testing of nuclear weapons to preserve the environment [6]. Despite this, several countries have improved their ability to launch a nuclear attack, such as North Korea, who performed a series of intercontinental missile tests in 2017.

To understand the factors determining the severity of a GMD or HEMP, we must review how these phenomena translate into grid impacts. First, GMDs and HEMPs cause disturbances in earth's magnetic field. These magnetic field fluctuations interact with the conductivity of the earth, creating an electric field at the earth's surface which induces a slowly-varying dc voltage across a power grid's transmission lines. Wye-grounded transformer windings create a path for unwanted dc currents, called geomagnetically induced currents (GIC), to flow throughout the power grid. When GIC flow through a transformer, it imposes a dc-offset on the ac waveform normally seen by the transformer. This causes the transformer to saturate every half cycle, negatively affecting the power grid by generating harmonics, heating transformers, and increasing the amount of reactive power absorbed by the transformer. This chain of causation is depicted in Fig. 1.

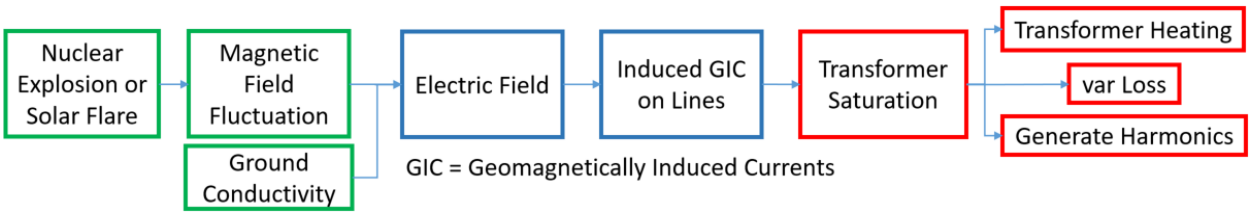

Fig. 1 How a GMD or HEMP negatively impacts the power grid

Although GMDs and HEMPs affect the electric grid through similar mechanisms, there are a few characteristics that distinguish a GMD from a HEMP. Unlike GMDs, HEMPs create electric fields at the earth's surface consisting of three consecutive components, called E1, E2, and E3. The E1 component occurs first, potentially having a peak magnitude measured in millions of volts per kilometer (V/km) and a duration measured in nanoseconds [7]. Because of its high magnitudes, the E1 electric field component has the potential to damage small electronics and communication devices [8].

The E2 component occurs next, having a magnitude of thousands of V/km and a duration measured in microseconds. According to [9], the effect of the E2 component has been compared to the impact of many small lightning strikes distributed across a large area. Its effect on the electric grid depends on the potentially weakened condition of the lightning protection equipment after the E1 and the initial capacity of the equipment to handle such a widespread disturbance.

Occurring last, the E3 component can be characterized by magnitudes on the order of tens of volts per km and has a duration which is measured in seconds. The E3 component has grid impacts like that of a GMD, but at a slightly faster timescale and higher magnitude [10]. Fig. 2 describes the relative duration and magnitudes of each of these components.

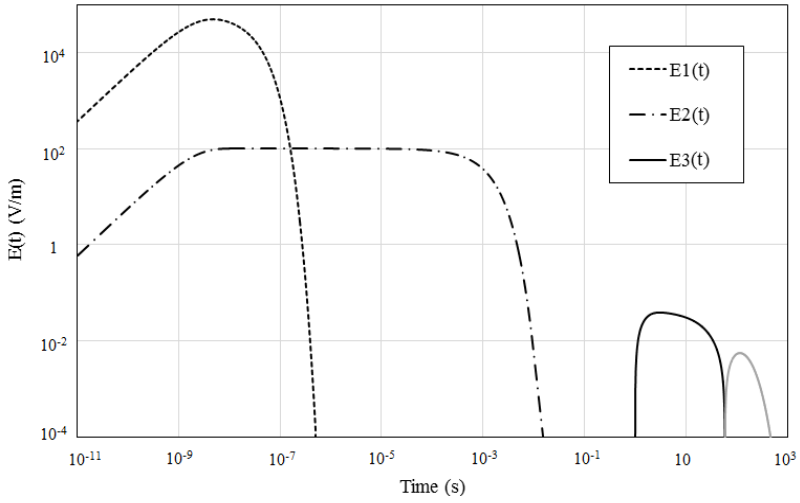

Fig. 2 Scale of magnitude and duration of E1, E2, E3 HEMP components from [7]

The timescale of each component determines how their effects are simulated on a power grid. The E1 and E2 components fall under the timeframe of an electromagnetic transients simulation while the E3's timeframe is suitable for transient stability [11]. Because of this, each component is frequently analyzed separately. This research presented in this document focuses only on the E3 component.

The magnitude of the electric field caused by a HEMP or GMD is highly dependent on the conductivity of the earth, hundreds of kilometers beneath the surface. The actual composition of the earth's conductivity is complex and different models are used to represent it. The uniform conductivity model is the simplest representation which assumes the entire earth has a single value of conductivity. Fig. 3 describes the 1D conductivity model which assumes the earth is made of flat layers of varying thicknesses and conductivity levels. In the figure, d_n and σ_n are depth and conductivity, respectively, of the n^{th} layer from the surface. The 1D model has not been used frequently to calculate HEMP electric fields. The only known work to do this is [12], which describes a method that converts the electric field from [7] to an electric field calculated under a

2-layer 1D model. Reference [13] uses data from geological surveys to define 1D conductivity profiles of regions across the continental United States, shown in Fig. 4.

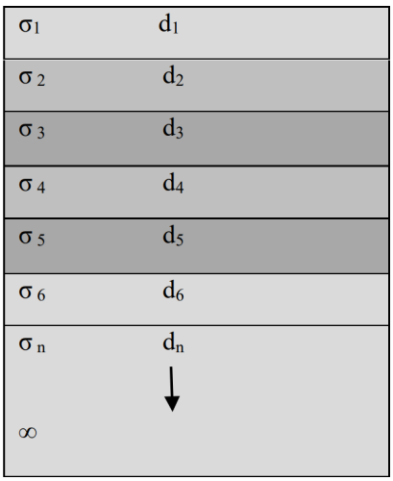

Fig. 3 1D conductivity model description from [14]

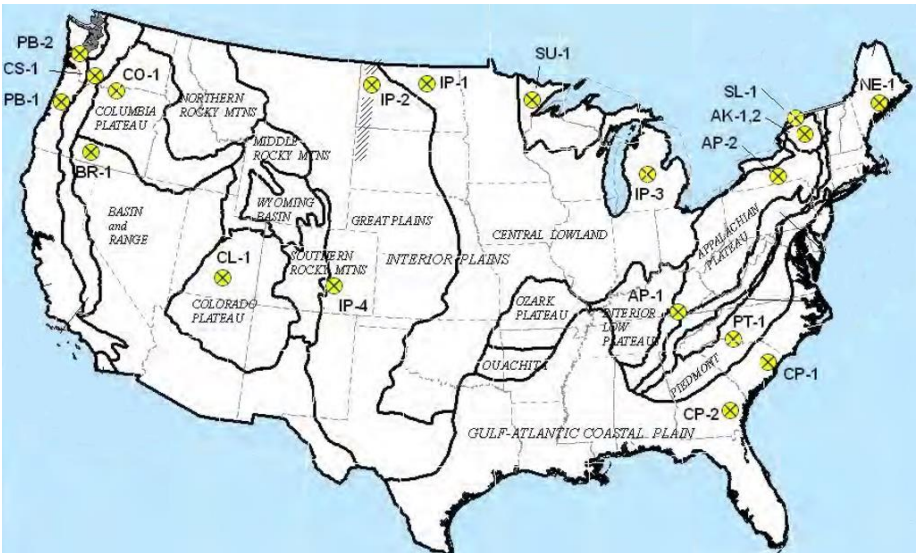

Fig. 4 1D conductivity regions as shown in [13]

Publicly available HEMP electric fields are often published under the uniform conductivity model. This document will describe an algorithm which converts these electric fields under the more realistic 1D conductivity model. Using this algorithm, I find HEMP electric fields for specific

geographic areas can be calculated, and the impact of a HEMP on electric grids can be evaluated with greater accuracy.

The motivation behind this work is to improve current capabilities to assess a power grid's vulnerability to a HEMP attack. NERC has published a standard requiring transmission planers to perform a periodic vulnerability assessment of their power grid to a GMD [15]. This standard describes a GMD electric field waveform, as shown in Fig. 5, developed using magnetometer measurements of the 1989 Quebec event.

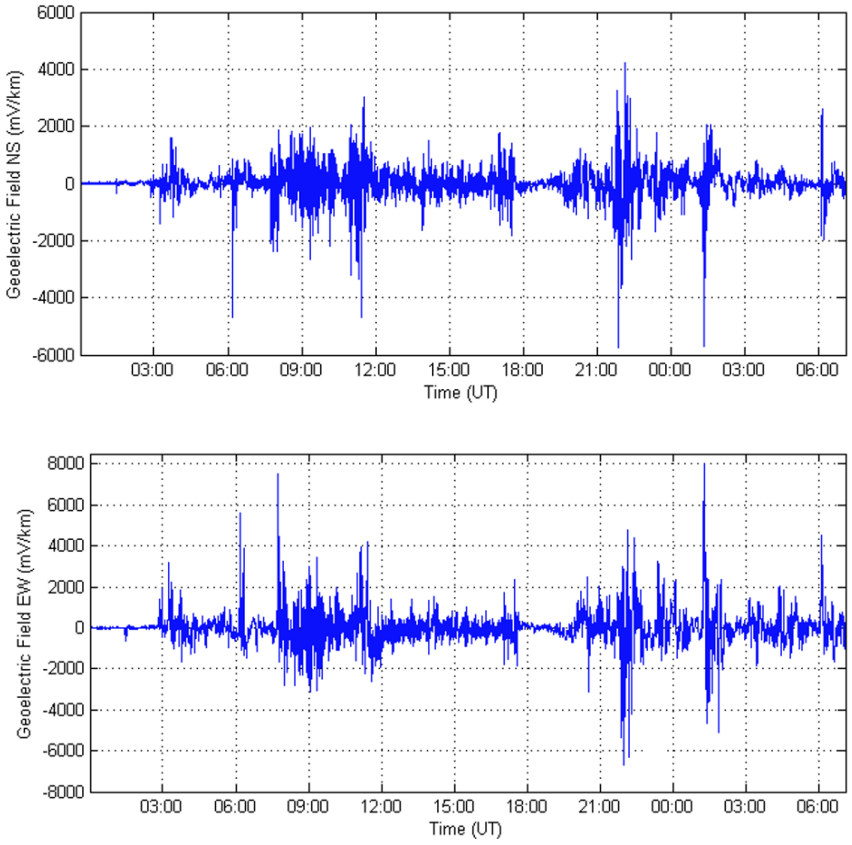

Fig. 5 Benchmark GMD electric field waveform from [15]

There currently exists no benchmark waveform or standard for reliability coordinators to evaluate their system to a HEMP event. By improving our understanding of the effects of publicly available HEMP electric field waveforms on an electric grid, this thesis aims to contribute toward the development of this type of standard using the method described in the previous paragraph.

Section 2 will cover previous work pertaining to the simulation of GIC on a power system. Section 3 provides a detailed explanation of the method used to convert publicly available HEMP electric fields under the uniform model to the 1D model. Section 4 compares the electric fields resulting from both conductivity models and evaluates their impact to a power grid using a 10,000-bus synthetic case. Section 5 summarizes the main points and reemphasizes key recommendations.

2. BACKGROUND* **

To understand the key contributions of this work, it is helpful to review previous work about E3 HEMP electric fields and their effect on electric grids.

A. Determining the Impact of an Electric Field on a Power Grid

If the electric field at the earth's surface is known, its impact on a power grid's voltage stability can be determined by calculating the flows of GIC throughout the network. To do this, the dc voltage induced on the transmission lines, V_{dc}, is calculated using Faraday's law [16]. The electric field, *E*, is integrated along the path of the transmission line using (1) where $\bar{dl}$ is the incremental length of the line.

$$V_{dc} = \oint E \cdot \bar{dl} \tag{1}$$

The dc bus voltages are then estimated using (2) where **I** is the Norton equivalent injection currents vector calculated from V_{dc}. **G** is the conductance matrix of the system which has been augmented to include substation grounding resistance values. **V** is a vector containing the substation neutral dc voltages and bus dc voltages.

$$\mathbf{V} = \mathbf{G^{-1}I} \tag{2}$$

With the bus dc voltages known, Ohm's law can be used to obtain the GIC flowing through the transmission lines and transformers. The effective GIC, $I_{GIC,pu}$, is calculated next which scales the per unit GIC flowing through each transformer depending on its winding configuration such as a grounded wye-delta or autotransformer.

Equation (3) is used to calculate $Q_{loss,pu}$, the reactive power absorbed by the transformer due to $I_{GIC,pu}$. K is a scaling factor which depends on the transformer's core type and the number of phases and limbs. V_{pu} is the transformer's high side ac voltage in per unit [17].

$$Q_{loss,pu} = V_{pu} K I_{GIC,pu} \tag{3}$$

The base value for $Q_{loss,pu}$ is determined using (4) from [18], where $V_{high,rated}$ is the rated voltage of the high side of the transformer. The base value for $I_{GIC,pu}$ is the rated current on the high-side of the transformer, $I_{high,rated}$.

$$Q_{base} = \sqrt{3} V_{high,rated} I_{high,rated} \tag{4}$$

The voltages across the system can be calculated by including Q_{loss} into the model as a constant current reactive load at the transformer buses [10].

Rise times of HEMP electric fields are on the order of seconds. I capture dynamics associated with stalling induction motors with simulations performed using transient stability [19].

B. Publicly Available Electric Fields

Researchers have primarily used two publicly available HEMP electric fields to evaluate the potential impact of a HEMP on power systems [20] - [22]. In 1985, Oak Ridge National Labs (ORNL) published [23] describing the time-varying and spatially-varying electric field resulting

from an experimental nuclear bomb detonation. Fig. 6 describes the spatial characteristics of the waveform while the purple dashed line in Fig. 7 illustrates the waveform's time-varying characteristics.

Eleven years later, the International Electrotechnical Commission (IEC) published [7] describing a time-varying electric field with no details about spatial variation. This waveform is represented with a blue dot-dashed line in Fig. 7.

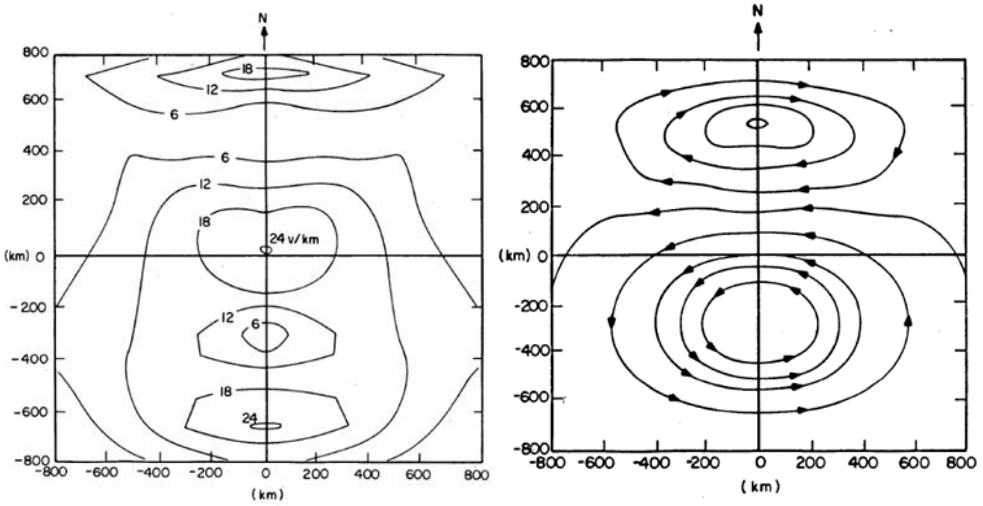

Fig. 6 HEMP electric field's spatial variation from [23]

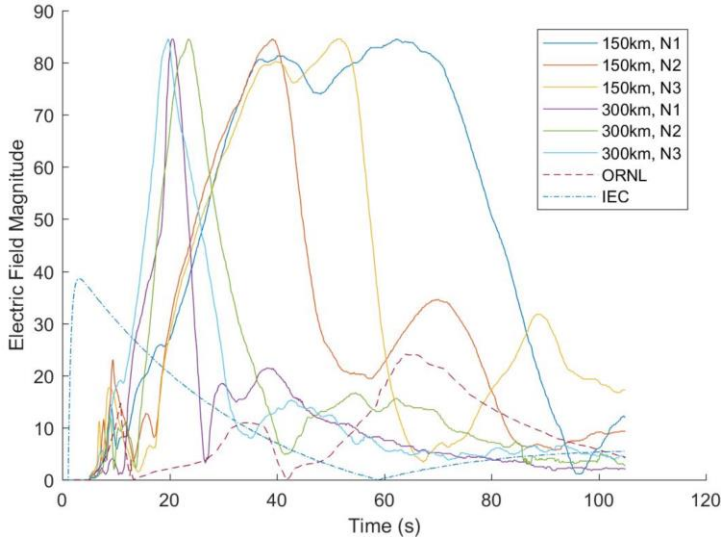

Fig. 7 Time-varying component of publicly available HEMP waveforms

More recently, [24] was released, describing the results of two high altitude nuclear tests conducted by the Soviet Union in 1962. The two detonations occurred at altitudes of 150 km and 300 km and have spatial characteristics which are shown in Fig. 8 on the left and right, respectively. The magnetic field of each blast was measured at three locations at the earth's surface called N1, N2, and N3. Using these data, six electric field waveforms were calculated. Considering the proximity of the measurements to the peak location of the HEMP and that the electric field is greater at lower geographic latitudes, [24] suggested using a peak electric field of 84.57 V/km for studies performed in the United States. Fig. 7 depicts the six electric field waveforms after they have been normalized to their peak magnitude and multiplied by 84.57 V/km.

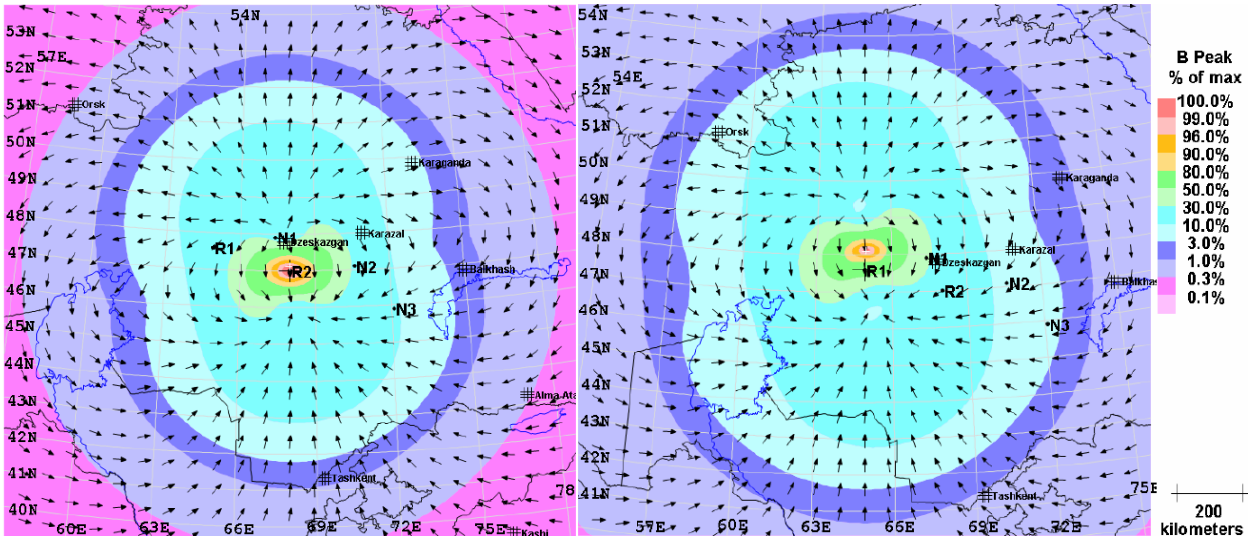

Fig. 8 Spatial variation of HEMP magnetic field from [24]

The publicly available electric field waveforms mentioned above, from [7][23][24], are all calculated under the uniform conductivity model, with conductivity values of 10^{-4}, 10^{-3}, and 10^{-3} Siemens per meter (S/m), respectively.

C. Validity of the 1D Model

The 1D model has been commonly used to simulate GIC induced by GMDs caused by solar activity [25]-[30]. In [28]-[30], the authors used magnetometer data collected in the field and a 1D ground conductivity model to simulate the flow of GIC in the neutral of a transformer during a period of high geomagnetic activity. The high correlation found between field and simulated data of these GMD events motivates the application of a 1D conductivity model to a HEMP simulation.

Fig. 9 describes two plots from [30] showing a highly correlated time series of simulated versus measured GIC flowing through different transformers during a period of high geomagnetic activity in May 2016.

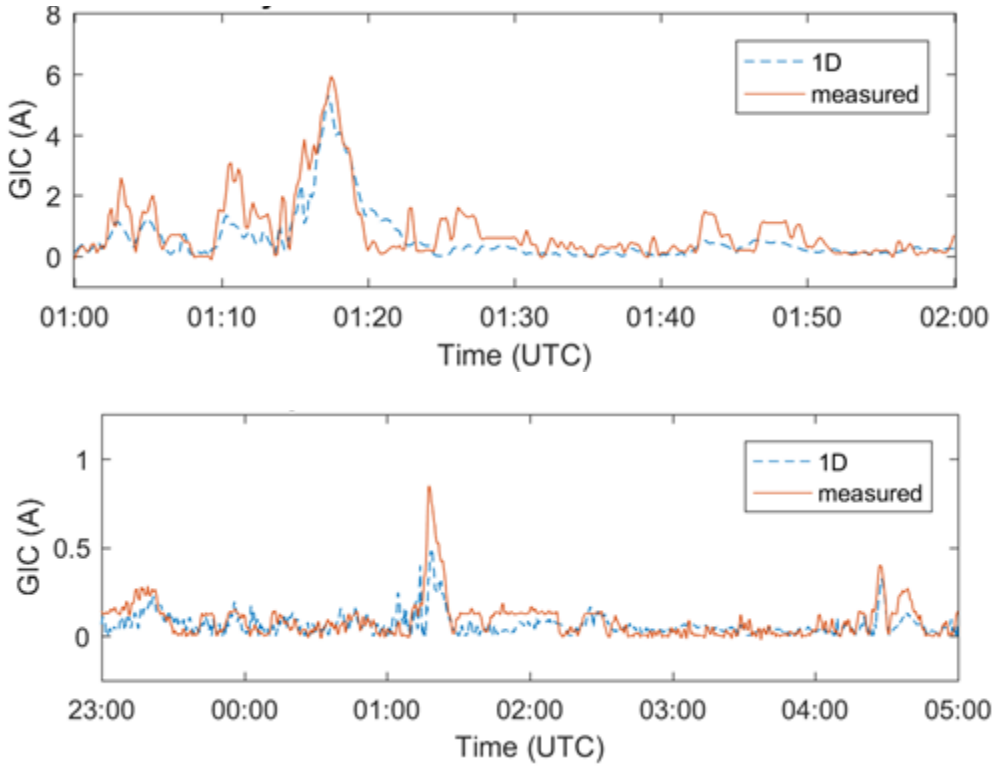

Fig. 9 Simulated vs. measured transformer neutral GIC flow, from [30]

3. METHODOLOGY – APPLYING 1D MODEL TO HEMP ELECTRIC FIELDS*

A block diagram of the algorithm used to convert an electric field between the uniform and 1D conductivity models is described in Fig. 10. This method will be used in this thesis to apply the 1D conductivity model to publicly available HEMP electric field waveforms at different locations in the United States.

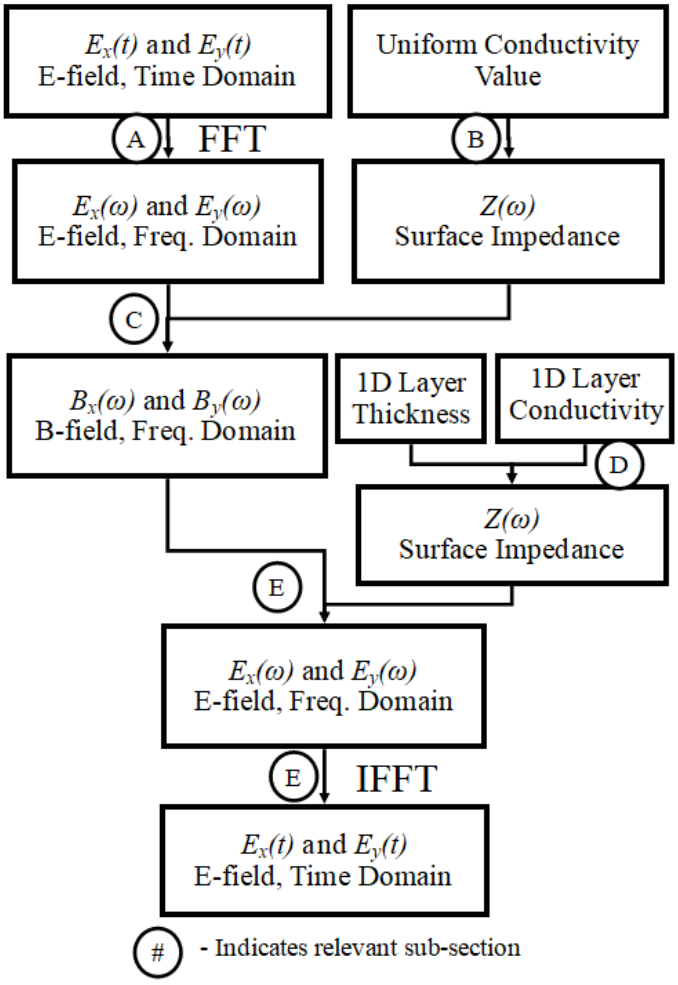

Fig. 10 Algorithm to convert HEMP electric field from uniform to 1D model

To help explain the algorithm, this section will include an example calculation starting with the electric field from [23], estimated under the uniform conductivity model of 10^{-3} Siemens/meter, and converting it under the "Pacific Border – 2" (PB-2) 1D conductivity profile, described in Fig. 11.

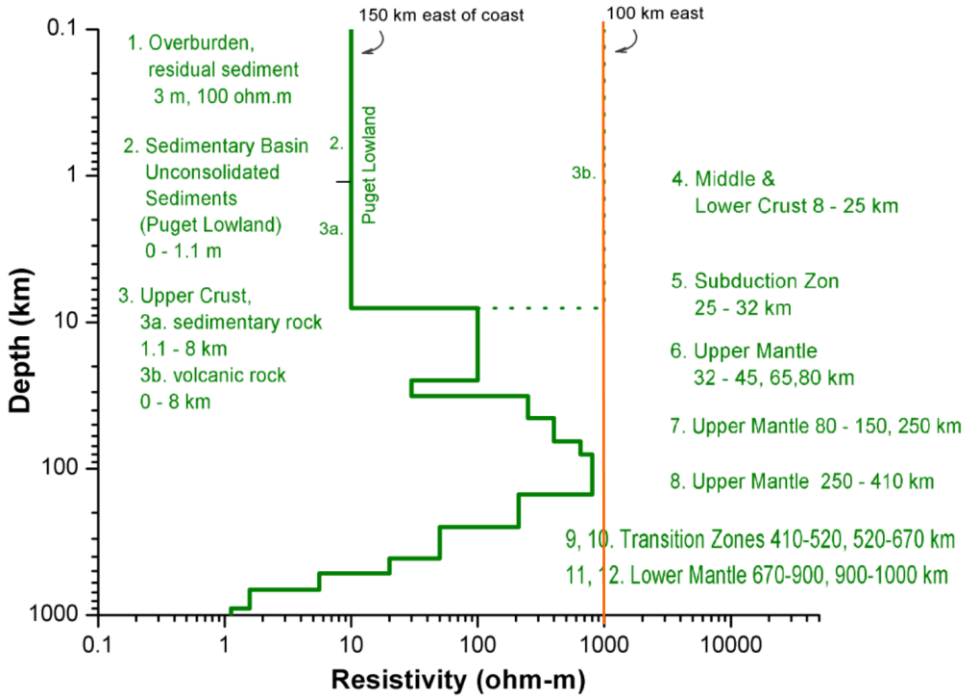

Fig. 11 Uniform resistivity (orange) and 1D resistivity (green) for region PB-2 from [13]

The electric field from [23] can be described as spatially-varying over a rectangular area of 2600 km by 2400 km. If one assumes a 25 km resolution, this can be represented by a 104 by 96-point grid. The algorithm described in Fig. 10 must be applied to each of these points independently to convert the entire electric field from the uniform model to the 1D model. As an example, this section will show calculations for one of these points at which the electric field has only an east-west component.

A. Obtaining $E(\omega)$

One of the inputs to the algorithm is the time series electric field, $E(t)$, calculated under the uniform conductivity model. As mentioned earlier, the electric field from ORNL will be used as an example during this section. The solid blue line in Fig. 12 describes its time-varying characteristics. Performing an FFT will convert the electric field from the time domain to the frequency domain as required by (5) and (6).

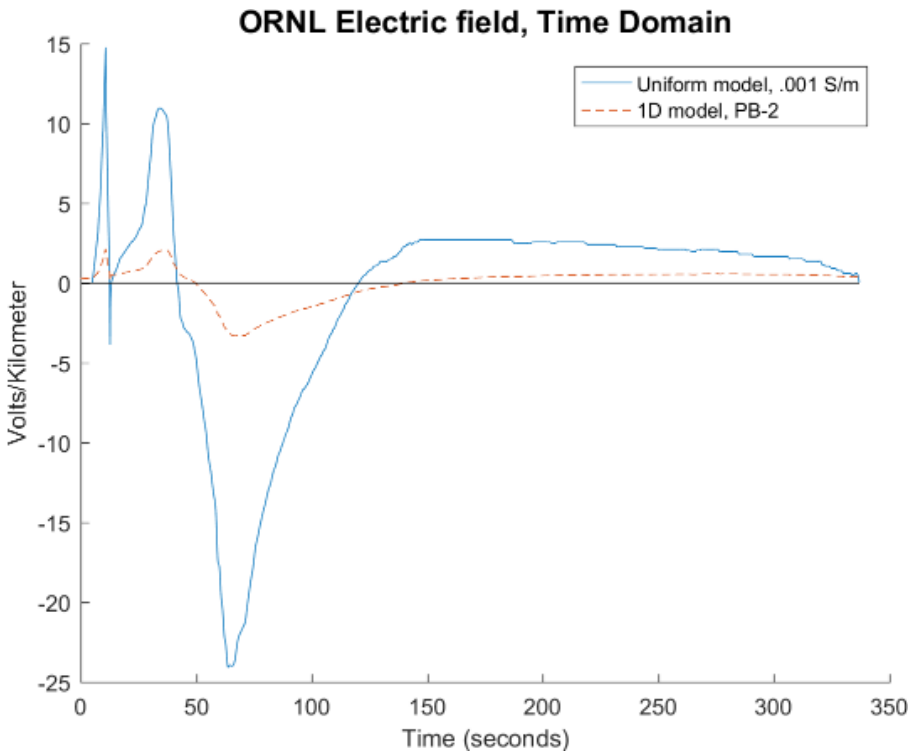

Fig. 12 ORNL electric field in the time domain

$$E_x(\omega) = \frac{-Z(\omega)B_y(\omega)}{\mu_0} \tag{5}$$

$$E_y(\omega) = \frac{Z(\omega)B_x(\omega)}{\mu_0} \tag{6}$$

E	electric field magnitude;
Z	surface impedance;
B	magnetic flux density;
μ_0	magnetic permeability of free space;
x	northern direction;
y	eastern direction;
ω	angular frequency;

The result of the FFT is illustrated using the solid blue line in Fig. 13. The frequencies .0089 Hz, .0445 Hz, and .0801 Hz were selected to show the results of the calculations involved in the algorithm at each step and are circled in Fig. 13. These results are summarized in Table 1.

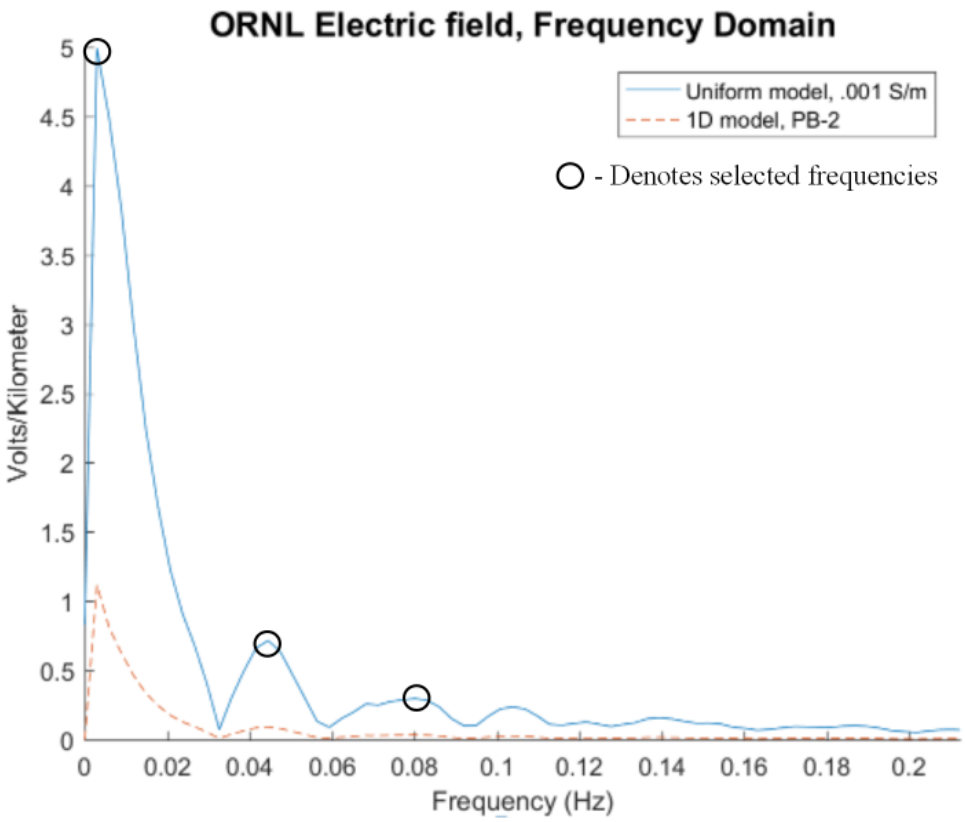

Fig. 13 ORNL electric field in the frequency domain

B. *Obtaining Z(ω) From Uniform Conductivity Model*

The uniform conductivity model assumes that the material underneath the surface of the earth has a single value of conductivity, σ. Equation (7) is used to calculate Z(ω), using the uniform conductivity model, for each value of ω [14].

$$Z(\omega) = \frac{\sqrt{j\omega\mu_0}}{\sigma} \tag{7}$$

C. *Obtaining $B(\omega)$*

Knowing $E(\omega)$ and Z(ω), (5) and (6) can be used to calculate $B(\omega)$. This calculation must be performed for each value of ω [27].

D. *Obtaining Z(ω) From 1D Conductivity Model*

Given the depth and conductivity of each layer of the 1D ground model, the surface impedance, *Z(ω)*, can be calculated using the method described in [14].

Each layer has a propagation constant, k_n, estimated using (8) where n is the layer number, starting with 1 as the bottom layer, and σ_n is the conductivity of the layer in Siemens/meter.

$$k_n = \sqrt{j\omega\mu_0\sigma_n} \tag{8}$$

The impedance of the bottom layer, Z_n, as seen at the surface, can be calculated using (9).

$$Z_n = \frac{j\omega\mu_0}{k_n} \tag{9}$$

To calculate the impedance of the layer above, a reflection coefficient, r_{n+1}, must be calculated using (10).

$$r_n = \frac{1-k_n\frac{Z_{n+1}}{j\omega\mu_0}}{1+k_n\frac{Z_{n+1}}{j\omega\mu_0}} \tag{10}$$

The impedance of the layer above, as seen at the surface, can be calculated using (11) where d_n is the thickness of the nth layer.

$$Z_n = j\omega\mu_0\left(\frac{1-r_n e^{-2k_n d_n}}{k_n(1+r_n e^{-2k_n d_n})}\right) \tag{11}$$

The process of using (10) and (11) must be continued iteratively for each layer until the surface of the earth is reached to get the final surface impedance value for the entire set of conductivity layers.

To obtain Z(ω), the surface impedance calculation must be done for each value of ω.

E. Obtaining E(ω) and E(t) Under 1D Conductivity Model

To obtain E(ω), (5) and (6) need to be invoked again, except this time using Z(ω), calculated under the 1D conductivity model. An inverse FFT can be used to convert the electric field from the frequency domain to the time domain to obtain E(t).

The orange dotted lines in Fig. 12 and Fig. 13 show the ORNL electric field, converted under the PB-2 1D conductivity profile. Comparing the two waveforms on Fig. 12, the 1D model produced a peak electric field 7.2 times smaller than the uniform model. Observing the results in rows A and E in Table 1, the electric field at each frequency decreased by different amounts when converted to the 1D model. The amount of change at each frequency is dictated by the differences in *Z(ω)*, between the uniform and 1D models, depicted in Fig. 14.

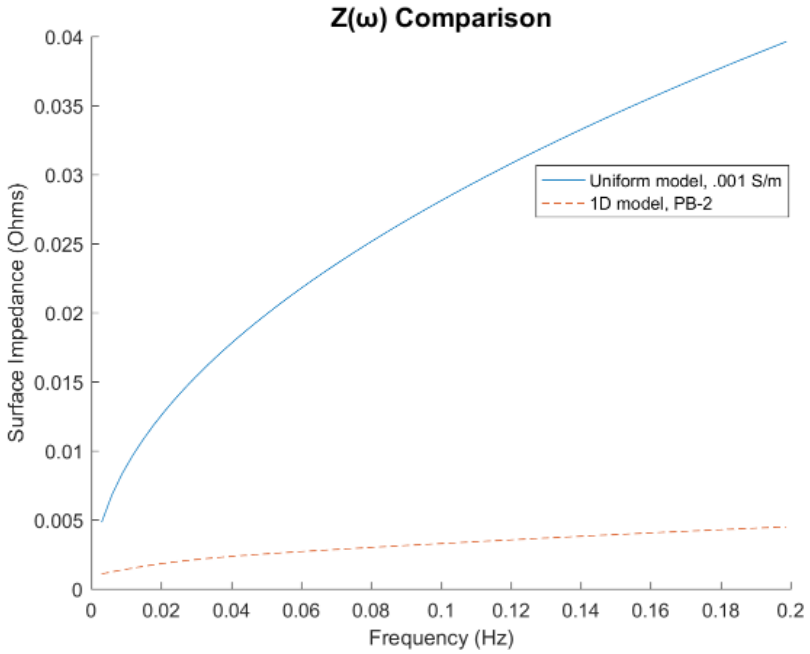

Fig. 14 Surface impedance in the frequency domain

Table 1 – Example Calculation Results

	Frequency (Hz)	.0030	.0445	.0801
A	**Electric Field Magnitude (Volts/km) Uniform Conductivity, .001 Siemens/meter**	4.992 (-0.799+j4.93)	0.7180 (-0.697-j0.17)	0.2985 (0.0475+j0.2947)
B	**Surface Impedance (Ohms) Uniform Conductivity, .001 Siemens/meter**	0.0034 +j0.0034	0.0133 +j0.0133	0.0178 +j0.0178
C	**Magnetic Flux Density (Teslas)**	$(-8.0-j11)*10^{-4}$	$(4.1-j2.5)*10^{-5}$	$(-12.1+j8.7)*10^{-6}$
D	**Surface Impedance (Ohms) 1D Conductivity, PB-2 Region**	0.0010 +j0.0004	0.002 +j0.0013	0.0024 +j0.0017
E	**Electric Field Magnitude (Volts/km) 1D Conductivity, PB-2 Region**	1.1168 (0.264+j1.09)	0.0933 (-0.093-j0.027)	0.0356 (0.012+j0.034)

(#) - Indicates relevant sub-section

F. Algorithm Automation Using MATLAB

A MATLAB tool was developed to automate this method. A screenshot of the user interface is shown in Fig. 15. This tool enables the user to calculate publicly available HEMP electric fields under the 1D conductivity model at any latitude and longitude in the continental United States. The resulting electric field is converted to a binary file format called ".b3d". Powerworld's GIC module can read the .b3d file to apply the electric field to a power systems simulation.

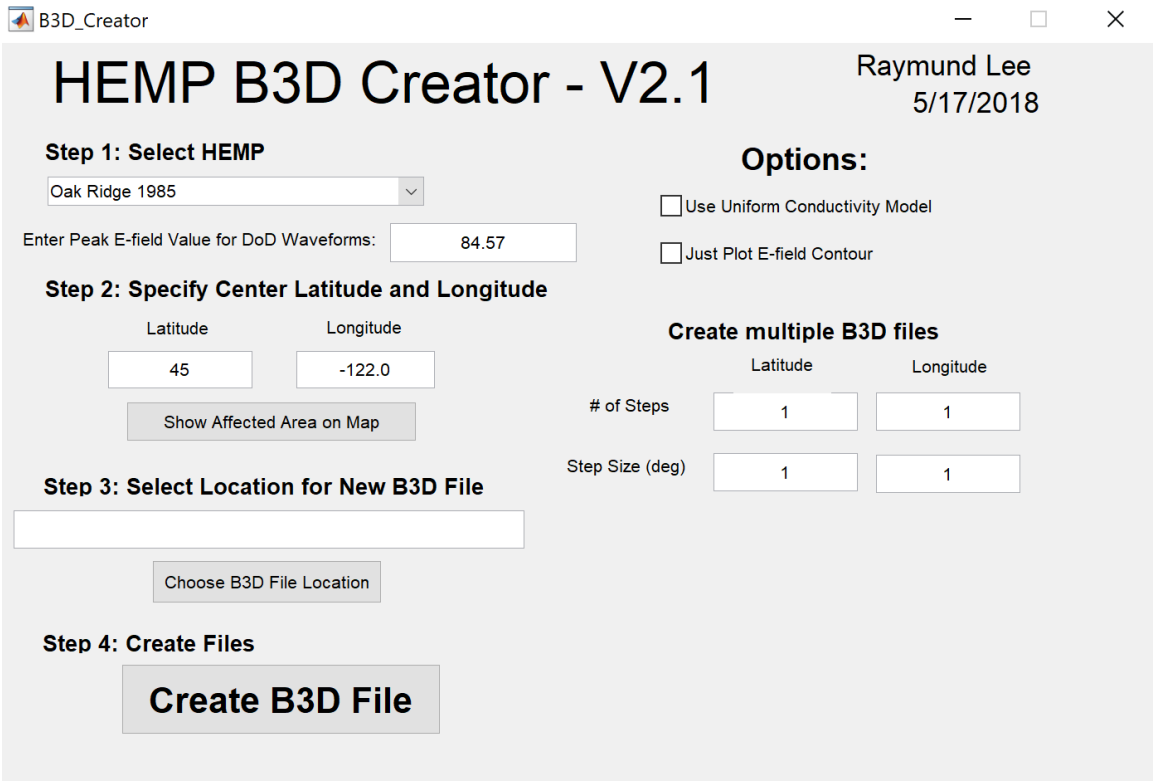

Fig. 15 User interface of HEMP calculator developed using MATLAB

4. ANALYSIS AND RESULTS* **

This section describes how the simulated impact of different HEMP electric field waveforms changes drastically depending on the conductivity profile used to calculate the electric field. First, the 1D conductivity model will be applied to the HEMP electric field from [23] at two different locations in the continental United States. Next, the peak magnitude of each publicly available HEMP waveform, as described in Fig. 4, will be determined for each 1D conductivity region defined by [13]. Finally, the impact of each publicly available waveform on a power system will be analyzed using a 10,000 bus synthetic case.

A. Uniform versus 1D model – Electric Field Magnitudes

Fig. 16 depicts the ORNL electric field under the uniform model when it is at its peak magnitude. As mentioned earlier, the ORNL HEMP's geographic footprint was discretized into a 104 x 96 grid of points. To convert the entire electric field under the 1D model, each of these points needs to be mapped to a geographic location by selecting the HEMP's center latitude and longitude. The calculations described in Section III must be done independently for each of these points. It is essential to note that the 1D conductivity region may differ from one point to another. First, a center of 45°N, -122°W was selected. The electric field magnitudes resulting from the conversion are shown in Fig. 17.

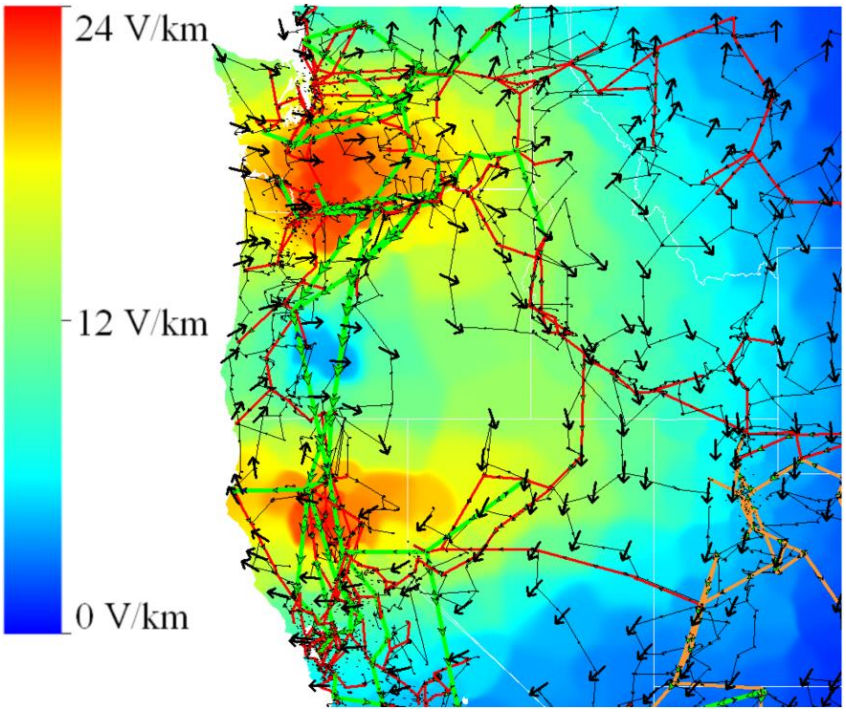

Fig. 16 Electric field contour of HEMP centered on (45,-122), uniform model

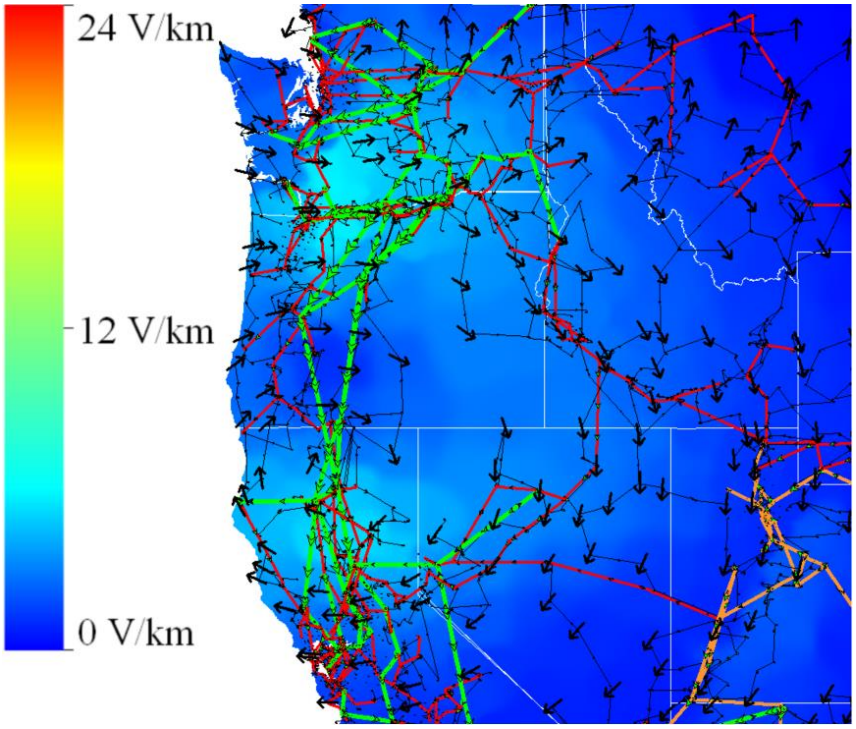

Fig. 17 Electric field contour of HEMP centered on (45,-122), 1D model

There are significant differences between the HEMP electric field magnitudes shown in Fig. 16 and Fig. 17. These contours use the same color scale to highlight the significantly reduced electric fields in Fig. 17. These figures display the electric field magnitude when it is at its maximum intensity. In Fig. 16, the electric field shown has three distinct peaks - the top peak, middle peak, and bottom peak. The top peak has a magnitude of 19 V/km while the middle peak and bottom peak have a magnitude of 24 V/km. In contrast, in Fig. 17, the top, middle, and bottom peaks have much lower magnitudes of 3.382 V/km, 5.061 V/km, and 5.416 V/km respectively.

These differences can be explained by analyzing the resistivity profiles of each conductivity model. The 1D conductivity regions of the western United States; PB-1, PB-2, CS-1, CO-1, and BR-1; do not exceed 10^3 Ohms/meter at all depths [13]. As an example, the 1D resistivity profile of PB-2 is represented in Fig. 4 using green lines and the uniform resistivity of 10^3 Ohms/meter used by [23] is represented using orange lines. From (5) and (6), the electric field calculated under the 1D model in these western regions is expected to be weaker than one calculated with a uniform conductivity of 10^{-3} Siemens/meter.

The 1D model does not always yield a weaker electric field than the uniform model. Fig. 18 describes the electric field for a HEMP with a center latitude and longitude of 29°N, -97°W. In this figure, there is an abrupt change in electric field magnitude dividing the eastern and western areas of Texas. This boundary is caused by the differences in resistivity between the western and eastern conductivity regions of Texas. The southeastern region of Texas, called "Coastal Plains – 2" (CP-2), has a resistivity profile described in Fig. 19. It is not apparent whether the resulting electric field for region CP-2 is lower than the uniform model since the third, fourth, and fifth layers from the surface of the 1D model have a higher resistivity. After performing the calculations

described in Section III, it was determined that region CP-2 generates a peak electric field of 31.8 V/km, which is higher than the peak electric field under the uniform model.

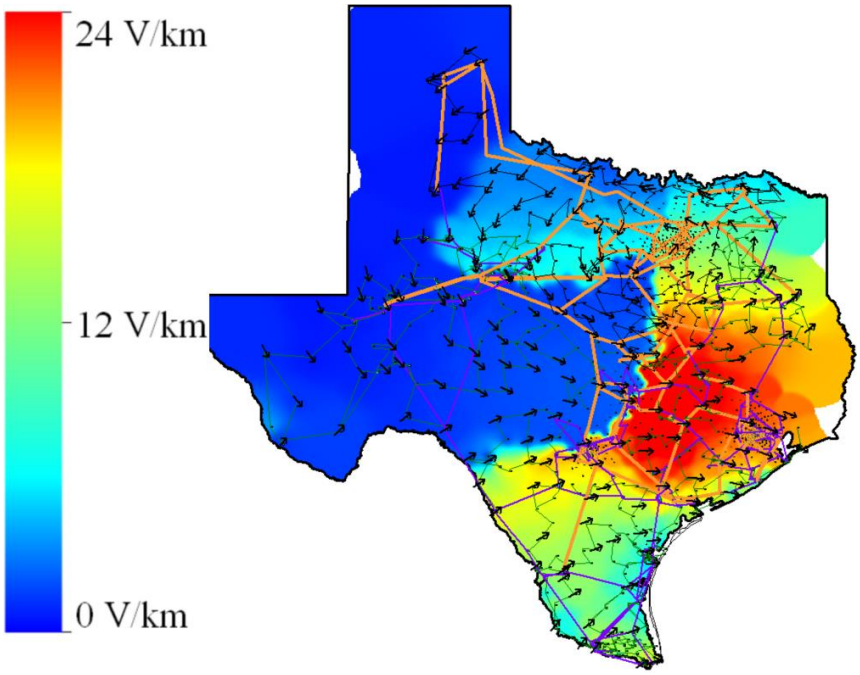

Fig. 18 Electric field contour of HEMP centered on (29,-97), 1D model

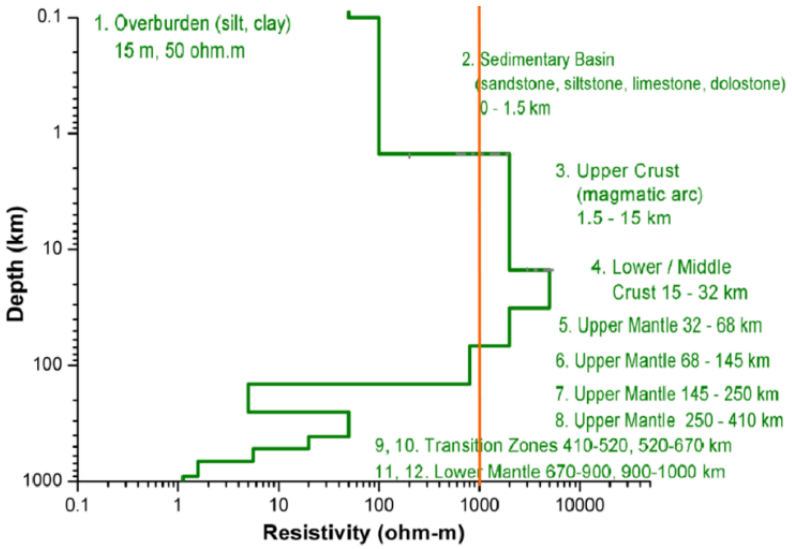

Fig. 19 Uniform resistivity (orange) and 1D resistivity (green) for region CP-2 from [13]

B. The Effect of 1D Regions on Electric Field Magnitude

In this section, the electric field waveforms from Fig. 7 were converted under each 1D conductivity region to observe how their peak magnitude would vary. Table 2 summarizes the results of this exercise.

Table 2 – Peak Electric Field (V/km) of Each HEMP Waveform per Conductivity Region

Conductivity Region	*150km, N1*	*150km, N2*	*150km, N3*	*300km, N1*	*300km, N2*	*300km, N3*	*ORNL*	*IEC*
IP-4	9.93	8.58	9.74	6.41	7.13	6.71	2.43	1.17
PB-2	13.11	12.39	13.15	10.88	11.39	11.11	3.33	1.59
IP-2	16.25	15.73	15.58	20.63	19.63	20.11	4.89	3.25
BR-1	17.17	17.08	17.17	14.97	16.17	15.67	4.90	2.16
CO-1	18.06	18.51	17.73	19.14	19.37	19.35	5.36	2.75
AP-1	19.57	19.57	19.03	22.63	21.70	22.12	5.82	3.42
CS-1	19.67	20.37	19.52	20.80	21.50	21.31	5.76	3.06
PB-1	22.11	20.18	21.95	16.22	17.77	16.95	5.58	2.60
SL-1	30.90	29.65	29.35	46.45	37.50	40.63	9.50	9.23
AK-1	31.43	30.32	30.92	47.69	37.94	41.15	9.80	9.59
CL-1	44.80	45.08	44.93	45.06	45.99	45.82	12.90	6.75
NE-1	53.99	53.95	52.51	63.60	58.03	59.90	16.37	10.02
IP-1	56.07	50.40	55.19	37.46	42.43	39.61	14.42	6.27
AP-2	56.26	56.39	54.67	64.59	60.62	61.89	16.98	9.93
IP-3	59.79	57.32	59.54	49.35	52.71	51.20	16.29	7.12
SU-1	60.77	60.22	60.47	62.12	59.30	59.52	17.44	9.31
CP-1	70.51	65.57	69.20	53.27	58.26	56.04	19.03	7.85
10^{-3} Siemens/m	**84.57**	**84.57**	**84.57**	**84.57**	**84.57**	**84.57**	**24.00**	12.2
PT-1	101.14	97.05	100.28	82.80	89.11	86.29	27.91	11.97
CP-2	107.86	109.04	105.31	104.77	112.32	109.20	31.80	14.93

The most important observations to take away from the results in Table 2 are outlined in the following paragraphs:

1. **Applying one waveform to different regions can yield greatly differing magnitudes**

In two regions, CP-2 and PT-1, the peak electric fields were calculated using the 1D model were higher than the electric field calculated using a uniform conductivity of 10^{-3} S/m. The only

exception is the peak electric field for the IEC waveforms under region PT-1. In all other regions, the 1D model yielded a lower electric field.

Comparing the extremes of the 1D regions, for waveform “300km, N1”, the peak electric field calculated under region CP-2 is over 16 times larger than if it were estimated under region IP-4. Also, the peak electric field, for this waveform, under 1D region IP-4, is 13.19 times smaller than if it were calculated under a uniform conductivity of 10^{-3} S/m.

Electric grids can span thousands of miles and cover a geographic footprint whose conductivity varies drastically. By assuming a uniform conductivity throughout the entire footprint, an E3 HEMP simulation is subject to high levels of inaccuracy.

2. **Waveforms with similar magnitudes under the uniform model can be affected much differently under the same 1D region**

The rows in Table 2 were sorted by putting the values in column “150km, N1” in descending order. It is important to observe that the other columns are not necessarily sorted in descending order, showing that each 1D conductivity region has a different effect on each waveform. This can be seen by comparing region SL-1’s effect on each electric field waveform. The waveforms yielding the highest and lowest electric fields are “300km, N1” and “150km, N3”, which have peaks of 46.45 V/km and 29.35 V/km, respectively. Despite having the same peak electric field of 84.57 V/km under the uniform conductivity model, the resulting peak electric fields under the same 1D conductivity model can be very different. Waveform “300km, N1” may yield the largest peak electric field in region SL-1; however, it yields the lowest peak electric field for region IP-1, out of the six waveforms from [24].

Developing an effective benchmark electric field waveform to assess the vulnerability of a power grid to HEMP requires an understanding of the worst-case scenario. The significance of this

observation is that the worst-case waveform for one region may not be the worst-case waveform for another region.

The following subsections will illustrate how the variations in conductivity regions and waveforms, mentioned earlier, can affect the results of an E3 HEMP simulation on a power grid.

C. Comparing Grid Impacts Between the Uniform and 1D Models

To illustrate how differently they impact an electric grid, the HEMP electric field from [23] under the uniform and 1D models were evaluated using a 10,000 bus synthetic grid [31][32]. This fictitious grid was developed using statistical analysis of real large-scale interconnected grids and was validated against models of real systems [33].

As mentioned in Section 1, GIC affects the grid by causing transformers to saturate. Two grid impacts of GIC are evaluated: transformer hot spot heating and voltage instability due to increased reactive power absorption.

1. Transformer Hot Spot Heating

Half-cycle saturation causes magnetic flux to leak from the transformer's core, inducing eddy currents on metallic components of the transformer such as the tie-plate and the windings [34]. This results in heating and potential damage of these components [35].

NERC standard [15] requires transmission planners to perform a thermal study on transformers that exceed 75 amps per phase (A/ph) of effective GIC during a GMD simulation. Transformers that do not exceed 75 A/ph of effective GIC are considered safe from hot spot damage. The justification for using 75 A/ph as a conservative screening criterion can be found in [36].

There are 2381 transformers in the 10,000 bus synthetic grid. 103 transformers exceeded 75 A/ph of effective GIC when the HEMP under the uniform model was applied to the grid. In this scenario, the largest effective GIC magnitude seen by a transformer was 342 A/ph. This transformer stayed above 75 A/ph of effective GIC for 49.8 seconds. In contrast, when applying the HEMP under the 1D model, no transformers exceeded 75 A/ph of effective GIC. The highest levels of effective GIC flowing through transformers in each of these scenarios are described in Fig. 20.

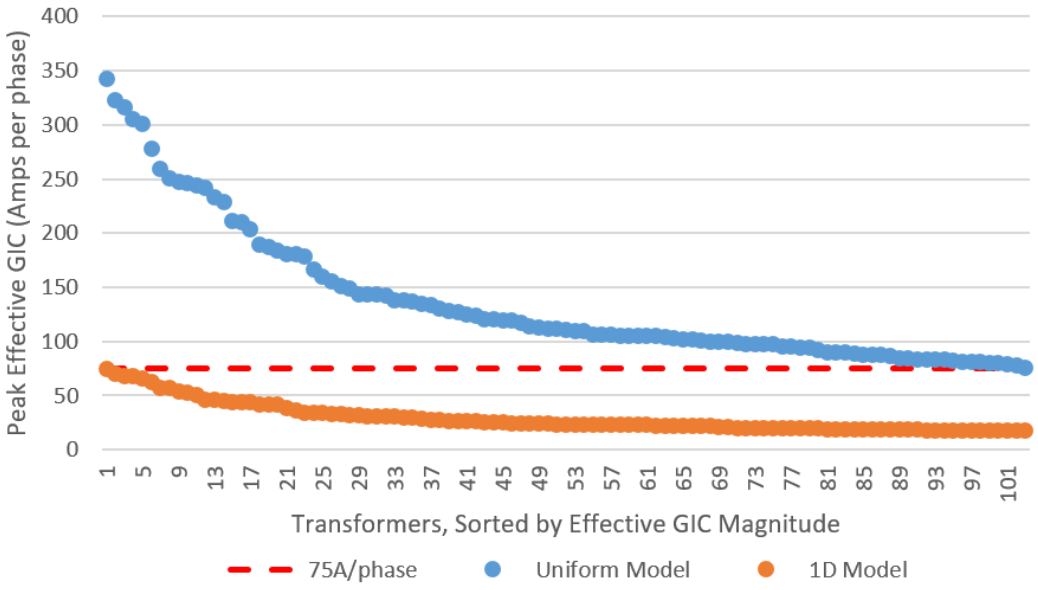

Fig. 20 Transformers with the highest levels of effective GIC

2. Voltage Instability Due to Reactive Power Loss

Increased reactive power absorption, leading to voltage sag, is another effect of transformer half-cycle saturation. To evaluate the voltage stability of the 10,000 bus case, a CLOD load model was used throughout the system with 25% large motors, 25% small motors, 20% discharge lighting, and 30% constant current [37].

The system-wide peak amount of reactive power absorbed by transformers due to GIC is 7,981 Mvar and 36,254 Mvar for the 1D model and uniform model, respectively. The difference in impact to the grid can be observed by comparing Fig. 21 and Fig. 22 which describe the maximum voltage deviation caused by the HEMP under each conductivity model.

Fig. 23 is a time series plot of voltage for a 345kV bus in the heavily impacted area on the west side of the 10,000 bus system. At this bus, the initial voltage started at 1.03 pu. 63.25 seconds into the simulation, the voltage dropped to 0.8386 pu and 1.0053 pu under the uniform model and 1D model respectively. The fact that there was a more extreme voltage drop under the uniform model was expected due to the significantly faster rise-time and magnitude of reactive power absorbed by transformers under this model.

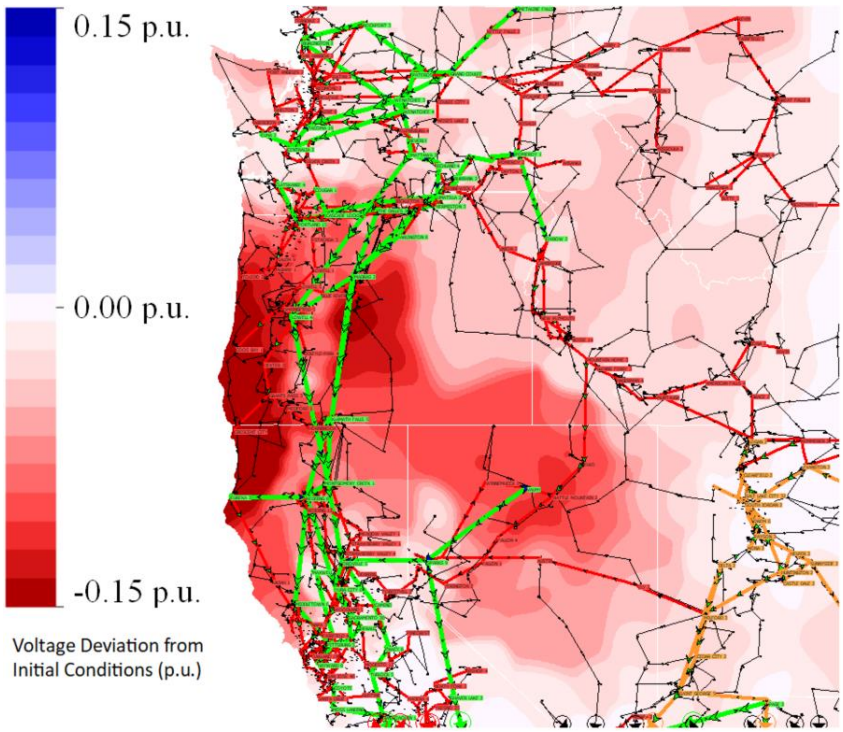

Fig. 21 Per unit voltage deviation at peak intensity, uniform model

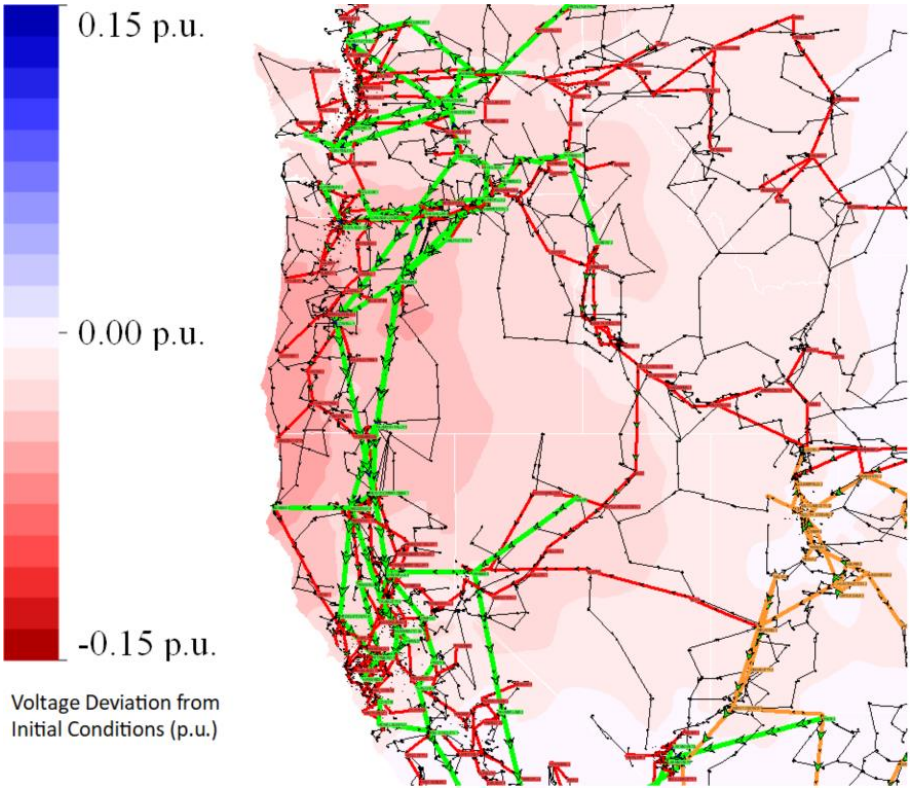

Fig. 22 Per unit voltage deviation at peak intensity, 1D model

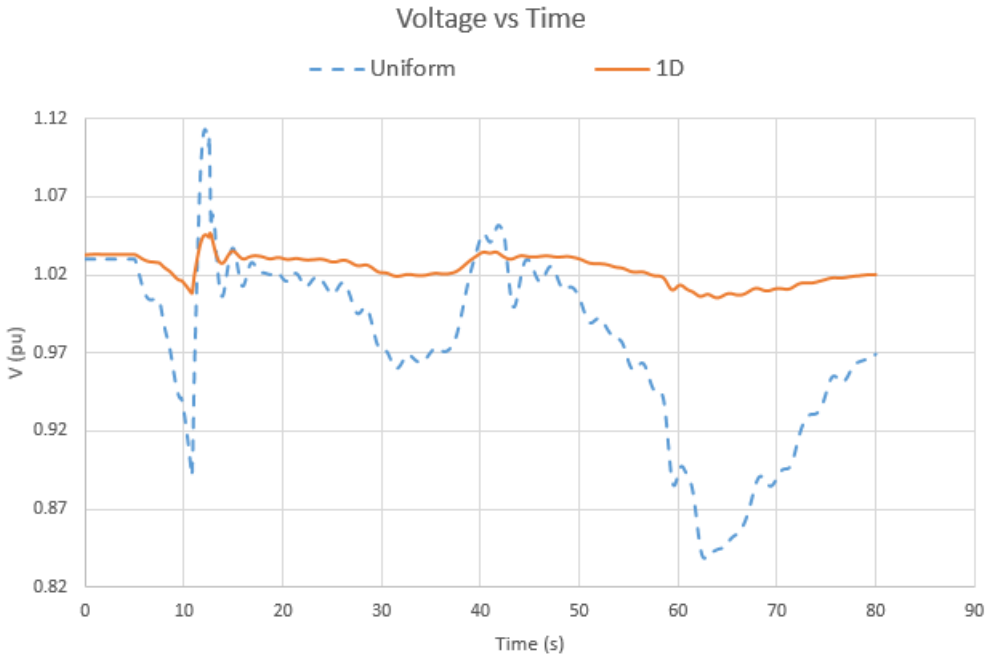

Fig. 23 Voltage fluctuations at a 345kV bus

D. Comparing Grid Impacts of Different HEMP Waveforms

This section evaluates the effect of each electric field waveform, published in [23] and [24] on the 10,000-bus synthetic grid introduced earlier. It is important to note that each waveform from [24] has a peak electric field magnitude of 84.57 V/km under the uniform model. The waveforms will vary as it is applied to the 1D regions associated with the footprint of the 10,000-bus synthetic grid. To quantify the impact of each waveform, two quantities will be observed: Voltage deviation from initial conditions and transformer effective GIC. Since [7] did not describe any details on the electric field's spatial characteristics, this waveform will be omitted from this section.

Five seconds into the simulation, each HEMP waveform was applied to the 10,000-bus synthetic grid at a center latitude and longitude of 46.1°N, -121.6°W. Fig. 24 depicts a contour of the "150km, N1" electric field magnitude when it is at its maximum intensity in relation to the circuit elements of the 10,000-bus synthetic case.

The results of this section are summarized in Table 3.

1. Voltage Instability Due to Reactive Power Loss

Fig. 25 is a plot of the voltage deviation from initial conditions of a 345kV bus. The "300km, N1" electric field produced the greatest voltage deviation while the "150km, N3" electric field produced the lowest. This result confirms previous work which concluded that fast electric field rise times yield higher levels of voltage deviation [10].

The ORNL waveform yielded a maximum voltage drop of only 0.0178 p.u. As expected, it had a much less severe impact on voltage stability compared to the six newer waveforms due to the sheer differences in electric field magnitude.

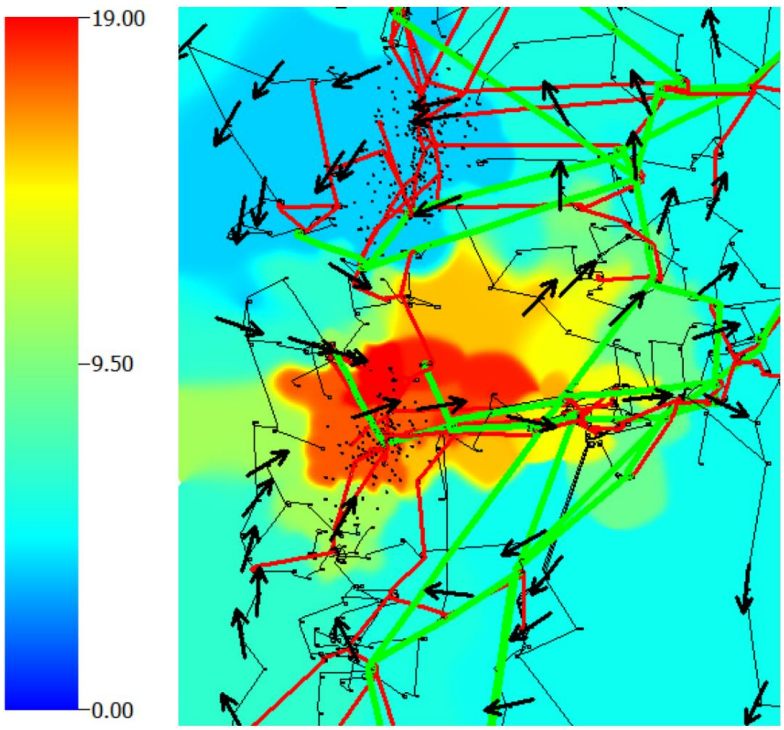

Fig. 24 "150km,N1" HEMP electric field magnitude at peak intensity

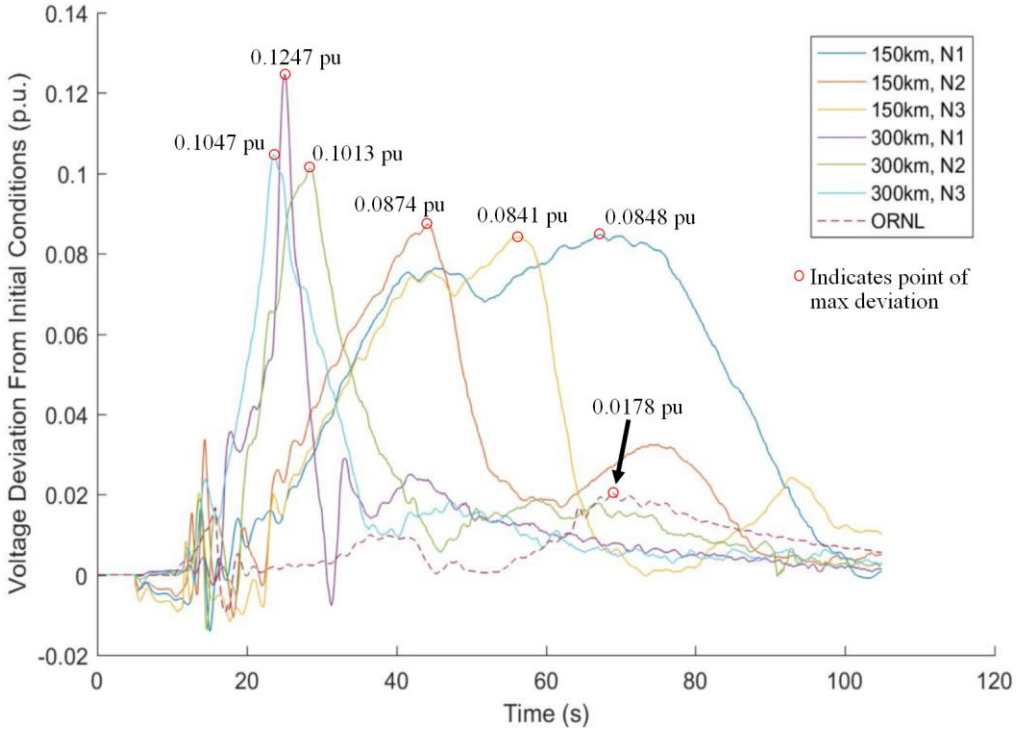

Fig. 25 345kV Bus' voltage deviation from initial conditions during HEMP simulations

2. Transformer Effective GIC

As mentioned previously, transformers which exceed 75 amps per phase (A/ph) of effective GIC are considered at-risk for damage due to transformer heating according to [15].

The amount of damage sustained by a transformer also depends on the length of time it is exposed to high heat. Furthermore, transformers take time to heat up when exposed to a certain level of effective GIC [35]. Therefore, it is also essential to analyze the length of time a transformer is exposed to high levels of effective GIC. The last row of Table 3 contains the length of time a specific transformer spent above 75 A/ph of effective GIC.

Interestingly, the three "300km" electric field waveform scenarios have the highest number of transformers reaching GIC levels above 75 A/ph. However, applying the "150km" waveforms caused the observed transformer to stay above 75 A/ph for a longer time. This is because the 150km waveforms have sustained levels of high electric field magnitude.

Table 3 – Comparison of Grid Impacts Using Different Waveforms

	150km, N1	*150km, N2*	*150km, N3*	*300km, N1*	*300km, N2*	*300km, N3*	*ORNL*
Max Voltage Deviation (p.u.)	0.0848	0.0874	0.0841	0.1247	0.1013	0.1047	0.0178
Number of Transformers I_{gic} > 75A/phase	24	23	24	31	33	33	8
Length of time I_{gic} >75A/phase (seconds)	71.83	59.87	75.43	10.36	20.58	17.4	0

5. SUMMARY AND CONCLUSION* **

To improve vulnerability assessments of a HEMP on a power grid, we introduced a method which converted a publicly available electric field calculated under a simple uniform conductivity model to a more realistic 1D conductivity model. The magnitude of the electric fields resulting from the 1D conductivity model varied greatly from region to region. The uniform conductivity model does not consider these regional differences. Since the 1D model is a more realistic representation of the conductivity of the earth than the uniform model, the use of the 1D model may be preferred when performing HEMP vulnerability studies on a real system. The 1D conductivity model has been tested in multiple papers such as [29] and [30], which conclude that transformer neutral currents measured in the field have a high correlation with values simulated with the 1D model.

The method that was introduced was used to analyze publicly available HEMP electric field waveforms by converting them to each conductivity region defined by [13]. By doing this, it was observed that different waveforms with the same peak magnitude under the uniform model, may have very different peak magnitudes when converted under the same 1D region.

The six new HEMP waveforms published by [24] were then applied to a simulation of a 10,000 synthetic grid. During the simulation, three waveforms yielded high voltage drop due to their high rise-times. The other three waveforms caused the observed transformer to stay above 75 A/ph of effective GIC for a longer period due to their sustained high levels of magnitude.

Completing a HEMP vulnerability assessment requires an understanding of the worst-case scenario. When selecting a waveform to conduct an assessment, it is important to consider how the waveform is affected by the power grid's local ground conductivity profile. Secondly, multiple waveforms may need to be used which have unique characteristics which yield different grid impacts such as voltage instability or transformer heating.

REFERENCES

[1] "High-Impact, Low-Frequency Event Risk to the North American Bulk Power System," North American Electric Reliability Corporation and the U.S. Department of Energy. Jun. 2010.

[2] R. Howard, B. J. LaBonte, "The Sun Is Observed To Be A Oscillator With a Period Of 11 Years," The Astrophysical Journal, vol. 239: L33-L36, 1980 July 1.

[3] "March 13, 1989 Geomagnetic Disturbance," NERC. Available: https://www.nerc.com/files/1989-Quebec-Disturbance.pdf

[4] J. G. Kappenman. "Great geomagnetic storms and extreme impulsive geomagnetic field disturbance events – An analysis of observational evidence including the great storm of May 1921," Advances in Space Research 38. p 188-199. Aug. 2005.

[5] C. N. Vittitoe. "Did High-Altitude EMP Cause the Hawaiian Streetlight Incident?" Sandia National Laboratories. Jun. 1989.

[6] "Treaty Banning Nuclear Weapon tests in the Atmosphere, in Outer Space, and Under Water," USSR-US-UK. Signed at Moscow, Aug. 1963. Available online: https://treaties.un.org/doc/Publication/UNTS/Volume%20480/volume-480-I-6964-English.pdf

[7] "IEC 61000-2-9 – Electromagnetic Compatibility (EMC) – Part 2: Environment – Section 9: Description of HEMP Environment – Radiated Disturbance. Basic EMC Publication," International Electrotechnical Commission. Feb. 19, 1996.

[8] W. A. Radasky. “The Potential of Three High Power Electromagnetic (HPEM) Threats on Smart Grids,” IEEE Electromagnetic Compatibility Magazine. Vol 1, Issue 2. Pg 107-110. Jul. 2012.

[9] J. S. Foster, E. Gielde, W. R. Graham, R. J. Hermann, H. M. Klupfel, R. L. Lawson, G. K. Soper, L. L. Wood, J. B. Woodard, “Report of the Commission to Assess the Threat to the United states from Electromagnetic Pulse (EMP) Attack,” EMP Commission. Apr. 2008.

[10] T. Hutchins, “Modeling, Simulation and Mitigation of the Impacts of the Late Time (E3) High-Altitude Electromagnetic Pulse on Power Systems.” 2016.

[11] P. W. Sauer and M. A. Pai, Power System Dynamics and Stability, Champaign, IL: Stripes Publishing L.L.C., 1997, p. 4

[12] J. Gilbert, J, Kappenman, W. Radasky, E. Savage, “The Late-Time (E3) High-Altitude Electromagnetic Pulse (HEMP) and Its Impact on the U.S. Power Grid,” Oak Ridge National Laboratory, Metatech Corporation, Jan. 2010.

[13] P. Fernberg, “One-Dimensional Earth Resistivity Models for Selected Areas of Continental United States & Alaska,” EPRI, Palo Alto, CA, Technical Results (1026430), 2012.

[14] "Application Guide: Computing Geomagnetically-Induced Current in the Bulk-Power System, " NERC, Dec. 2013. [Online]. Available: http://www.nerc.com/comm/PC/Geomagnetic%20Disturbance%20Task%20Force%20GMDTF%202013/GIC%20Application%20Guide%202 013-approved.pdf

[15] “TPL-007-2 - Transmission System Planned Performance for Geomagnetic Events,” National Electric Reliability Council. Nov. 2017.

[16] T. J. Overbye, T. R. Hutchins, K. S. Shetye, J. Weber, S. Dahman, “Integration of Geomagnetic Disturbance Modeling into the Power Flow: A Methodology for Large-Scale

System Studies," in *Proc. 2012 North American Power Symposium,* Champaign, IL, USA, Sep. 2012.

[17] X. Dong, Y. Liu, J.G. Kappenman, "Comparative Analysis of Exciting Current Harmonics and Reactive Power Consumption from GIC Saturated Transformers," IEEE 2001 Winter Meeting, Columbus, OH, Jan. 2001.

[18] K. S. Shetye, T. J. Overbye, "Parametric Steady-State Voltage Stability Assessment of Power Systems using Benchmark Scenarios of Geomagnetic Disturbances," Power and Energy Conference at Illinois. Feb. 2015.

[19] T. J. Overbye, K. S. Shetye, Y. Z. Hughes and J. D. Weber, "Preliminary Consideration of Voltage Stability Impacts of Geomagnetically Induced Currents," in Power and Energy Society General Meeting (PES), July 2013.

[20] G. B. Rackliffe, J. C. Crouse, J. R. Legro, V. J. Krause, "Simulation of Geomagnetic Currents Induced in a Power System by Magnetohydrodynamic Electromagnetic Pulses," Westinghouse Electric Corporation. IEEE Transactions on Power Delivery, Vol. 3, No. 1, pp. 392-397, Jan. 1988.

[21] A.P. Sakis Meliopoulos, G. J. Cokkinides, Mario Rabinowitz, "Comparison of SS-GIC and MHD-EMP-GIC Effects on Power Systems," IEEE Transactions on Power Delivery, Vol 9, No. 1, pp. 194-207, Jan. 1994.

[22] R. Horton, "Magnetohydrodynamic Electromagnetic Pulse Assessment of the Continental U.S. Electric Grid," Electric Power Research Institute. Feb. 2017.

[23] "Study to Assess the effects of Magnetohydrodynamic Electromagnetic Pulse on Electric Power System, Phase 1, Final Report," Martin Marietta Energy Systems Inc. Oak Ridge National Labs. 1985.

[24] “Recommended E3 HEMP Heave Electric Field Waveform for the Critical Infrastructures,” Jul. 2017. Web Link: http://www.dtic.mil/dtic/tr/fulltext/u2/1051494.pdf

[25] L. Marti, C. Yiu, A. Rezaei-Zare, D. Boteler, “Simulation of Geomagnetically Induced Currents With Piecewise Layered-Earth Models,” IEEE Transactions on Power Delivery, Vol 29, No. 4, pp. 1886-1893, Aug. 2014.

[26] K. Zheng, L. Trichtchenko, R. Pirjola, L. Liu, “Effects of Geophysical Parameters on GIC Illustrated by Benchmark Network Modeling,” IEEE Transactions on Power Delivery, Vol 28, No. 2, pp. 1183-1191, Apr. 2013.

[27] D.H. Boteler, “Geomagnetically Induced Currents: Present Knowledge and Future Research” IEEE Transactions on Power Delivery, Vol 9, No. 1, pp. 50-58, Jan. 1994.

[28] T. Halbedl, R. Bailey, G. Achleitner, H. Renner, R. Leonhardt, “Analysis of the Impact of Geomagnetic Disturbances on the Austrian Transmission Grid.” Power Systems Computation Conference. Dec. 2016.

[29] A. Pulkkinen. R. Pirjola, A. Viljanen. “Determination of Ground Conductivity and System Parameters for Modeling of Geomagnetically Induced Current Flow in Technological Systems.” Sept. 2007.

[30] K. S. Shetye, J. L. Gannon, A. B. Birchfield, R. H. Lee, T. J. Overbye, “Impact of 1D vs 3D Earth Conductivity Based Electric Fields on Geomagnetically Induced Currents,” Innovative Smart Grid Technologies Conference. Feb. 2019.

[31] A. B. Birchfield, T. Xu, K.M. Gegner, K.S. Shetye, T.J. Overbye, “ Grid Structural Characteristics as Validation Criteria for Synthetic Networks,” IEEE Transactions on Power Systems, vol. 32, no. 4, pp. 3258-3265, Jul. 2017.

[32] T. Xu, A. B. Birchfield, K. S. Shetye, T. J. Overbye, “Creation of Synthetic Electric Grid Models for Transient Stability Studies,” Bulk Power Systems Dynamics and Control Symposium (IREP 2017), Espinho, Portugal, September 2017.

[33] A. B. Birchfield, E. Schweitzer, M.H. Athari, T. Xu, T. J. Overbye, A. Scaglione, Z. Wang, “A metric-based validation process to assess the realism of synthetic power grids,” Energies, vol. 10, no. 1233, pp. 1-14, Aug. 2017.

[34] L. Marti, A. Rezaei-Zare, A. Narang, “Simulation of Transformer Hotspot Heating due to Geomagnetically Induced Currents,” IEEE Transactions on Power Delivery, vol. 28, no. 1, Jan. 2013.

[35] “Transformer Thermal Impact Assessment White Paper,” North American Electric Reliability Corporation. Dec. 2014.

[36] “Screening Criterion for Transformer Thermal Impact Assessment,” North American Electric Reliability Corporation. May. 2016.

[37] “Load Characteristic CLOD Complex Load Model,” Available: https://www.powerworld.com/WebHelp/Content/TransientModels_HTML/Load%20Characteristic%20CLOD.htm